Loss of TGF-β Signaling and PTEN Promotes Head and Neck Squamous Cell Carcinoma through Cellular Senescence Evasion and Cancer-related Inflammation

Yansong Bian, MD, PhD[1, 4], Bradford Hall*, MS[1], Zhi-Jun Sun*, DDS, MD[1], Alfredo Molinolo, MD[2], Wanjun Chen, MD[3], J. Silvio Gutkind, PhD[2], Carter Van Waes, MD, PhD[4], and Ashok B. Kulkarni, PhD[1]

[1]Functional Genomics Section, Laboratory of Cell and Developmental Biology, [2]Oral and Pharyngeal Cancer Branch, [3]Mucosal Immunity Section, Oral Immunity and Infection Branch, National Institute of Dental and Craniofacial Research, and [4]Tumor Biology Section, Head and Neck Surgery Branch, National Institute on Deafness and Other Communication Disorders, NIH, Bethesda, MD 20892

*** Both authors made equal contribution**

Supplementary Information

Supplementary Material and Methods

Generation of *Tgfbr1/Pten* 2cKO mice. *Tgfbr1* cKO mice (mixed genetic strains of FVB/N, C57BL/6, 129SV/J and CD1) (Larsson *et al*., 2001; Bian *et al*., 2009) were crossed with the *Pten*$^{flox/flox}$ mouse line (genetic strain 129SV/J) (Groszer *et al*., 2001) to generate mice heterozygous for both *Tgfbr1* flox and *Pten* foxp with *K14-CreER*^{tam} (*K14-CreER*^{tam}*;Tgfbr1*$^{f/+}$*;Pten*$^{f/+}$). The *Tgfbr1/Pten* 2cKO mice (*K14-CreER*^{tam}*;Tgfbr1*$^{f/f}$*;Pten*$^{f/f}$) were generated from crosses between *K14-CreER*^{tam}*;Tgfbr1*$^{f/+}$*;Pten*$^{f/+}$ and *Tgfbr1*$^{f/f}$*;Pten*$^{f/f}$ mice. All care was given in compliance with the National Institutes of Health guidelines on the use of laboratory and experimental animals, and the studies were approved by the National Institute of Dental and Craniofacial Research (NIDCR) Animal Care and Use Committee (ACUC). Littermates were genotyped at 1 week of age and grouped based on genotypes for the experiments. Tamoxifen (200 μl of 10 μg/μl in corn oil) was applied in the oral cavity of 3-month-old *Tgfbr1/Pten* 2cKO mice for 5 consecutive days to induce homozygous deletion of

Tgfbr1 and *Pten* in head and neck epithelia (Vasioukhin *et al*., 1999; Lu *et al*., 2006). Paired *K14-CreER^{tam};Tgfbr1$^{f/+}$;Pten$^{f/+}$* and *Tgfbr1$^{f/f}$;Pten$^{f/f}$* mice were also treated with the same dosage of tamoxifen as the controls. To study early premalignant lesions, mice from each group were dissected at 4 weeks after Tamoxifen treatment. Once tumors developed in the oral cavity, mice were switched to soft food and monitored daily. Tumor-bearing mice were euthanized when tumor diameter approached 2 cm in size, if tumors were ulcerated and bleeding, or if there was any sign of the mice suffering from pain or weight loss as a result of the tumors. Necropsy was performed on each euthanized mouse. Histological slides were prepared to identify primary tumors and metastases in the cervical lymph nodes, lungs, and brain. Head and neck tissues, including the buccal mucosa and tongue, as well as other tissues such as the ear, esophagus, and forestomach, were also dissected.

Histology, immunostaining, and BrdU labeling. All tissues were fixed overnight in buffered 4% paraformaldehyde, transferred to 70% ethanol, and embedded in paraffin. Five-micron sections were cut and stained with hematoxylin and eosin. Immunohistochemical staining (IHC) and quantifications of IHC slides were performed using a previously published method (Czerninski *et al*., 2009). For tissue array, two staining patterns were distinguished relative to the number of positive cells as well as the staining intensity of normal mucosa: 1) ++: no change in expression compared with normal mucosa tissues, and 2) +/-: reduced expression or loss of expression compared with normal mucosa tissues. Intratumoral microvessel density (iMVD) was determined as previously described (Weidner *et al*., 1991). The following antibodies were used for immunostaining: PTEN (138G6) antibody (Cell Signaling Technology, Danvers, MA) at 1:50; TGFBR1 (ab31013) antibody, CDKN1A (ab7960) antibody (Abcam, Cambridge, MA) at

1:200 dilution; phospho-Smad2 (Ser465/467) antibody (Millipore, Billerica, MA), CCND1 (sc-718) antibody (Santa Cruz Biotechnology, Inc., Santa Cruz, CA) at 1:500 dilution; mouse Ki-67 (TEC-3) antibody (DAKO, Carpentaria, CA), and phospho-Akt (Ser473) antibody (Cell Signaling Technology, Danvers, MA) at 1:100 dilution; F4/80 (BM8) antibody (Invitrogen, Camarillo, CA); CD11b (M1/70) antibody (BD Pharmingen, San Diego, CA), Gr-1 (RB6-8C5) antibody (BD Pharmingen, San Diego, CA) at 1:100; Sox2 (C70B1) antibody (Cell Signaling Technology, Danvers, MA), and Oct4 (GTX101497) antibody (GeneTex, Irvine, CA) at 1:100. For BrdU labeling, mice were injected i.p. with 50 mg/kg body weight of BrdU (Sigma, St. Louis, MO) in sterile 1XPBS 4 hours before biopsy. BrdUrd immunostaining was performed on paraformaldehyde-fixed tissue sections using rat anti-BrdU antibody (Accurate Chemical & Scientific Corp, Westbury, NY) at 1:100 dilution. For immunofluorescent staining after incubation with primary antibody, the slides were incubated with fluorophore-conjugated secondary antibodies with 4', 6'-diamidino-2-phenylidole (DAPI) (Jackson ImmunoResearch Laboratories, Inc, West Grove, PA) for 1 hour in the dark at room temperature. The primary antibodies included the following: Keratin 14 (K14) antibody (Covance, Emeryville, CA), CD44 (550538) antibody (BD Pharmingen, San Diego, CA), CD133 (AC133) antibody (eBioscience, San Diego, CA), CD31 (550274) antibody (BD Pharmingen, San Diego, CA), and Endoglin (CD105) antibody (R&D Systems, Minneapolis, MN), all at 1:50 dilution. Sodium borohydride and Sudan Black B (Sigma, St. Louis, MO) were used to reduce aldehyde and lipofuscin-induced fluorescence. Confocal microscopy images were obtained using a Zeiss LSM 510 NLO META confocal microscope (Zeiss, Thornwood, NY).

Terminal deoxyribonucleotidyl transferase-mediated dUTP nick end labeling assay. Terminal deoxyribonucleotidyl transferase-mediated dUTP nick end labeling (TUNEL) assay was performed on paraformaldehyde-fixed tissue sections using an In situ Apoptosis Detection Kit and following the directions of the manufacturer (TaKaRa, Shiga, Japan).

Senescence assay. Senescence-associated β-galactosidase staining kit (Cell Signaling Technology, Danvers, MA) was used following the manufacturer's protocol. Briefly, cryosections were fixed in fixing solution for 15 min, washed with PBS, and then incubated overnight with a staining solution that included 5-bromo-4-chloro-3-indolyl-h-D-galactopyranoside. Sections were counterstained with diluted eosin. Cells positive for the marker per field (10X magnification) were counted, and at least 5 fields per genotype were scored. The mean and SD were calculated for each genotype.

Assessment of Cre-mediated recombination. Cre-mediated recombination of *Tgfbr1*$^{f/f}$ and *Pten*$^{L/L}$ alleles was assessed by a PCR-based assay using mouse tail DNA. An amplicon was generated only when the *Tgfbr1*$^{f/f}$ or *Pten* allele had undergone *Cre*-mediated recombination (Larsson et al., 2001; Groszer et al., 2001).

Quantitative real-time PCR analysis. Total RNA was isolated from the buccal mucosa and tongue of the *Tgfbr1/Pten* 2cKO mice and controls (*Tgfbr1*$^{f/f}$*;Pten*$^{L/L}$ mice) by using Trizol and chloroform. To determine the *Tgfbr1* and *Pten* mRNA expression levels in head and neck epithelia, 1 μg of total RNA was used for RT-PCR analysis as described (Honjo *et al*., 2007). The quantitative real-time PCR (qRT-PCR) was done in triplicate using samples from 5 mice.

Mouse cytokine RT- PCR array. DNA-free total RNA was prepared by homogenizing tissue with a Qiashredder column and using the miRNeasy kit with DNase digestion (QIAGEN). RNA quality was analyzed using Bioanalyzer (Agilent) and 1% E-gel (Invitrogen). The mouse cytokine PCR array profiles the expression of 84 key cytokine genes (SABiosciences, PAMM-011, Frederick, MD) in 3 *Tgfbr1*$^{fl/fl}$ */Pten*$^{fl/fl}$ tongues compared with 3 *Tgfbr1/Pten* 2cKO tongue SCC from individual mice. For each sample, 500 ng total RNA were reverse transcribed with RT2 First Strand Kit (SABiosciences) and applied to PCR array plates. Plates were processed in a Bio-Rad Chrome 4 PCR System, using the same baseline and threshold cycle detection. Data were analyzed by using the web-based Gene Network Central Pro™ PCR Array Data Analysis software.

Flow cytometry analysis. Flow cytometry staining was performed as described previously (Liu *et al*., 2008). Briefly, lymphocytes were isolated from jugular lymph nodes and stained with the indicated antibodies for the surface markers and then subjected to flow cytometry analysis.

Western blot analysis. Proteins were extracted from tissues using T-PER reagent (Pierce, Rockford, IL) with a complete mini protease inhibitor cocktail (Roche, Branchburg, NJ). NuPAGE 4-12% Bis-Tris precast gel was used for electrophoresis on the XCell surelock Mini-Cell (Invitrogen, Carlsbad, CA). A total of 40 µg of protein from each sample were denatured and then loaded in each lane. Proteins were then transferred onto a PVDF membrane. The signals were visualized using a horseradish peroxidase-conjugated secondary antibody (Santa Cruz

Biotechnology, Inc., Santa Cruz, CA) followed by chemiluminescence detection (Pierce, Rockford, IL). Subsequently, all blots were re-incubated with anti-β-Actin antibody and developed similarly as loading controls. The following antibodies were used: TGFBR1 antibody (sc-398) (Santa Cruz Biotechnology, Santa Cruz, CA) at 1:200 dilution, Smad2 antibody (Zymed, San Francisco, CA), phospho-Smad2 (Ser465/467) antibody (Millipore, Billerica, MA), and PTEN antibody (R&D Systems, Inc., Minneapolis, MN) at 1:500 dilution; Akt antibody, phospho-Akt (Ser473) (D9E) antibody, EGF Receptor (D38B1) antibody, p44/42 MAPK (Erk1/2) antibody, and phospho-NF-kB p65 (Ser536) (93H1) antibody (Cell Signaling Technology, Danvers, MA) at 1:100 dilution; NF-kB p65 (C22B4) antibody and phospho-Stat3 (Tyr705) (D3A7) antibody (Cell Signaling Technology, Danvers, MA) at 1:2000; CDKN2D (Ab-1) antibody (Calbiochem, Gibbstown, NJ), CDKN1A (sc-397) antibody, and Id1 (sc-488) antibody (Santa Cruz Biotechnology, Santa Cruz, CA) at 1:200; Phospho-TAK1 (Thr184) antibody (#4537) (Cell Signaling Technology, Danvers, MA) at 1:1000; anti-TAK1 (# 07-263) (Millipore Billerica, MA) at 1:500; anti-SMAD7 polyclonal antibody (#PA1-41506) (Thermo Scientific Life Sciences, Rockford, IL) at 1:500; Phospho-NF-kB p65 (Ser536) (Cell Signaling Technology, Danvers, MA) at 1:1000; NF-κB p65 (#4764) (Cell Signaling Technology, Danvers, MA) at 1:2000; NF-kB p50 antibody and β-Actin antibody (MAB1501) (Millipore, Billerica, MA) at 1:5000.

Immunoprecipitation. A total of 100 μg of protein was diluted in a 200 μl volume of T-PER (Pierce, Rockford, IL) with a complete mini-protease inhibitor cocktail (Roche, Branchburg, NJ). Lysates were incubated with 4 μl Phospho-Akt (Ser473) antibody (#4060) (Cell Signaling Technology, Danvers, MA) at 1:50 for 2 hours at 4^{o}C. Then, 20 μl of Protein

A/G Plus-Agarose (sc-2003, Santa Cruz Biotechnology, Santa Cruz, CA) was added and the lysates were incubated overnight at 4^{o}C. The immunoprecipitates were collected by centrifugation at 1000xg for 1 min (4^{o}C) and washed twice with cold PBS. Proteins were denatured and run on a NuPAGE 4-12% Bis-Tris precast gel for electrophoresis on the XCell surelock Mini-Cell (Invitrogen, Carlsbad, CA). Proteins were then transferred onto a nitrocellulose membrane. The membrane was first incubated with Smad3 antibody (ab28379) (Abcam, Cambridge, MA) at 1:1000, then stripped and incubated with Phospho-Akt (1:2000). The signals were visualized using a horseradish peroxidase-conjugated secondary antibody (Santa Cruz Biotechnology, Inc., Santa Cruz, CA) followed by chemiluminescence detection (Pierce, Rockford, IL).

Supplemental Figure Legends

Supplemental Figure S1 Loss of *Tgfbr1* in head and neck epithelia, together with activation of the PTEN/PI3K/Akt pathway by *Pten* deletion, results in SCCs in mice with complete penetrance. (a and b) The tissue-specific deletion of *Pten*, together with *Tgfbr1* in mice head and neck epithelia, causes multiple hyperproliferative lesions as well as tumor lesions in ears, vibrissae, skin, and paws. (c and d) The histological pictures provide a view of the status of the squamous epithelium in the different genotypes. The arrows in the two pictures (frontal head sections) allow for a comparison between the normal squamous epithelium of the skin (arrow) in the rightmost image and the hyperplastic, pseudopapillary epithelium of the skin in the *Tgfbr1/Pten* 2KO mouse. A thickening of the epithelium of the mouth (arrow head) is also evident. The white arrow points to a frontal section of the tongue also covered with hyperplastic mucosa. (e) Loss of *Tgfbr1* and *Pten* in head and neck epithelia results in HNSCCs in mice with complete penetrance. Spontaneous tumors were also observed in 20.8% of *Pten* cKO mice and 9.7% of *Tgfbr1* cKO. Only 2 out of 38 (5.3%) *Tgfbr1* and *Pten* floxed homozygous control littermates developed tumors. No tumors developed in the heterozygous mice over the course of 1 year of observation after Tam treatment.

Supplemental Figure S2 Conditional deletion of *Tgfbr1* and *Pten* in head and neck epithelia after Tam treatment by recombination PCR analysis. The *Tgfbr1* and *Pten* genomic loci were targeted for recombination. Black arrows indicate positions of PCR primers. Black arrowheads indicate LoxP sites (a and c). Specific *Tgfbr1* and *Pten* deletion in head and neck epithelia of *Tgfbr1/Pten* 2cKO mice (b and d). Genomic DNA was extracted from major tissues 10 weeks

after Tam treatment. *Tgfbr1* and *Pten* deletion was detected in the buccal mucosa (BM) and tongue (Tg), as well as in the ear (Er) of the *Tgfbr1/Pten* 2cKO mice.

Supplemental Figure S3 Inactivation of TGF-β signaling and activation of PTEN/PI3K/Akt pathway in *Tgfbr1/Pten* 2cKO mice. (a) *Tgfbr1* and *Pten* mRNA were significantly reduced in the head and neck epithelia of *Tgfbr1/Pten* 2cKO mice by qRT-PCR (n=3). **, P<0.01. (b) Tgfbr1, p-Smad2, and Pten expression were reduced, while p-Akt was overexpressed in the tongue of *Tgfbr1/Pten* 2cKO mice by IHC. The dotted lines delineate the adjacent epithelial compartment. The changes in staining patterns are seen in the epithelium (above the dotted line), in which *Tgfbr1* and *Pten* were knocked out (magnification, 200X). Bar=100um. (c) Western blot analysis demonstrates that Tgfbr1, p-Smad2, and Pten were reduced, while p-Akt expression was increased in the buccal mucosa and tongue of *Tgfbr1/Pten* 2cKO mice compared to $Tgfbr1^{f/f}$ /$Pten^{f/f}$ mice.

Supplemental Figure S4 Loss of Tgfbr1 does not result in downregulation of Smad-independent signaling. Increased activation of TAK1 occurs in SCC tissues of *Tgfbr1/Pten* 2cKO mice where TGF-β signaling is abrogated. Although Tgfbr1 is lost, no significant changes could be seen in the levels of Smad7.

Supplemental Figure S5 Deletion of Tgfbr1 allows Smad3 to interact with activated Akt. Protein lysates from tissues of the *Tgfbr1/Pten* 2cKO mice were incubated with phospho-Akt (Ser473) antibody. Tissues include the buccal mucosa, tongue, and three squamous cell

carcinomas from the *Tgfbr1/Pten* 2cKO mice. Smad3 was pulled down with the immunoprecipitated activated Akt, suggesting that these two proteins interact without TGF-β signaling to induce phosphorylation and translocation of Smad3.

Supplemental Figure S6 Validations of the expression of important cytokines by q-PCR. *Il1α, Il1β, Tnfα, Cxcl1, Cxcl5*, and *Ptgs2* were significantly increased in SCCs of *Tgfbr1/Pten* 2cKO mice. **, $P<0.01$; ***, $P<0.001$.

Supplemental Figure S7 Reduction of effector T-cells and immune suppression in *Tgfbr1/Pten* 2cKO mice. Compared with their control littermates, *Tgfbr1/Pten* 2cKO mice showed significantly reduced amounts of $CD8^+$ effector T cells at the same time as the regulatory T-cells $CD4^+CD25^+Foxp3^+$ was increased, indicating the existence of immune suppression in *Tgfbr1/Pten* 2cKO mice.

Supplemental References

Bian Y, Terse A, Du J, Hall B, Molinolo A, Zhang P, et al. (2009). Progressive tumor formation in mice with conditional deletion of TGF-beta signaling in head and neck epithelia is associated with activation of the PI3K/Akt pathway. *Cancer Res* **69:**5918-26.

Czerninski R, Amornphimoltham P, Patel V, Molinolo AA, Gutkind JS. (2009). Targeting mammalian target of rapamycin by rapamycin prevents tumor progression in an oral-specific chemical carcinogenesis model. *Cancer Prev Res* **2:**27-36.

Groszer M, Erickson R, Scripture-Adams DD, Lesche R, Trumpp A, Zack JA, et al. (2001). Negative regulation of neural stem/progenitor cell proliferation by the Pten tumor suppressor gene in vivo. *Science* **294:**2186-9.

Honjo Y, Bian Y, Kawakami K, Molinolo A, Longenecker G, Boppana R, et al. (2007). TGF-beta receptor I conditional knockout mice develop spontaneous squamous cell carcinoma. *Cell Cycle* **6:**1360-6.

Larsson J, Goumans MJ, Sjöstrand LJ, van Rooijen MA, Ward D, Levéen P, et al. (2001). Abnormal angiogenesis but intact hematopoietic potential in TGF-beta type I receptor-deficient mice. *EMBO J* **20:**1663-73.

Liu Y, Zhang P, Li J, Kulkarni AB, Perruche S, Chen W. (2008). A critical function for TGF-beta signaling in the development of natural CD4+CD25+Foxp3+ regulatory T cells. *Nat Immunol* **9:**632-40.

Lu SL, Herrington H, Reh D, Weber S, Bornstein S, Wang D, et al. (2006). Loss of transforming growth factor-beta type II receptor promotes metastatic head-and-neck squamous cell carcinoma. *Genes Dev* **20:**1331-42.

Vasioukhin V, Degenstein L, Wise B, Fuchs E. (1999). The magical touch: genome targeting in epidermal stem cells induced by tamoxifen application to mouse skin. *Proc Natl Acad Sci U S A* **96:**8551-6.

Weidner N, Semple JP, Welch WR, Folkman J. (1991). Tumor angiogenesis and metastasis--correlation in invasive breast carcinoma. *N Engl J Med* **324:**1-8.

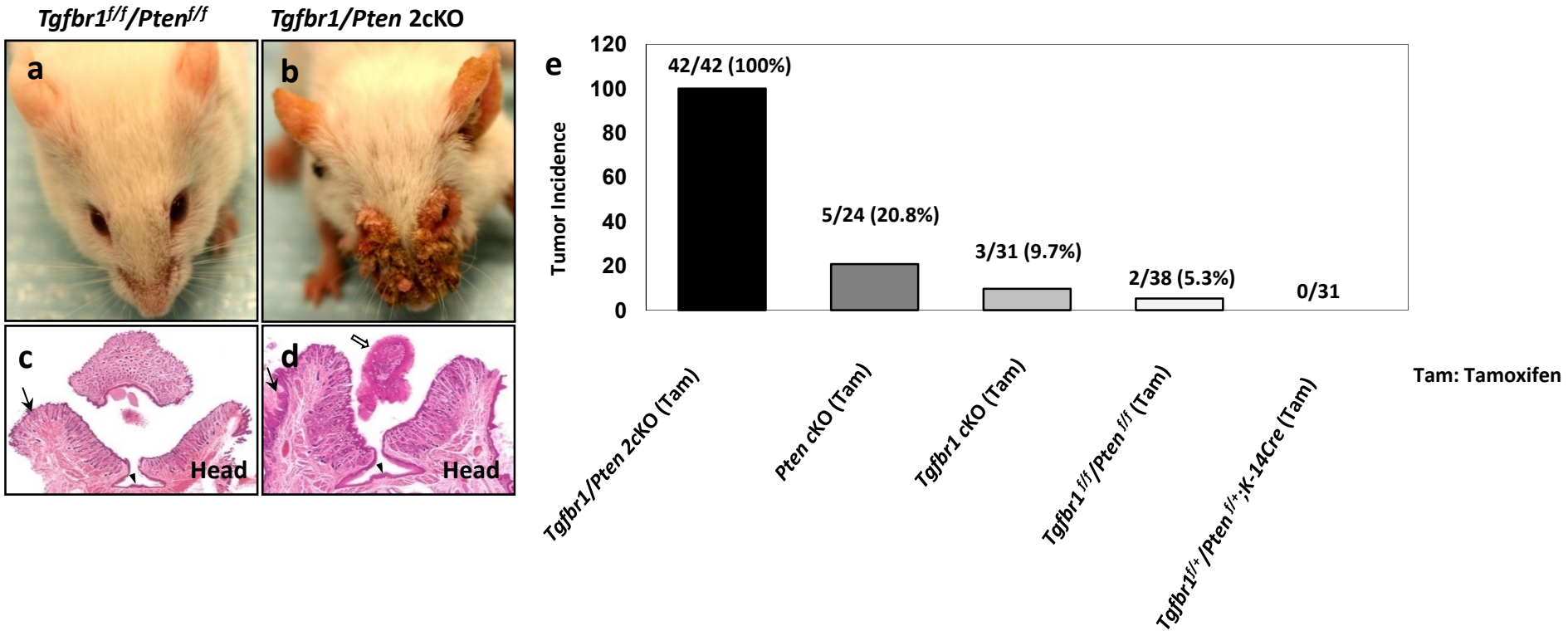

Supplemental Figure S1.

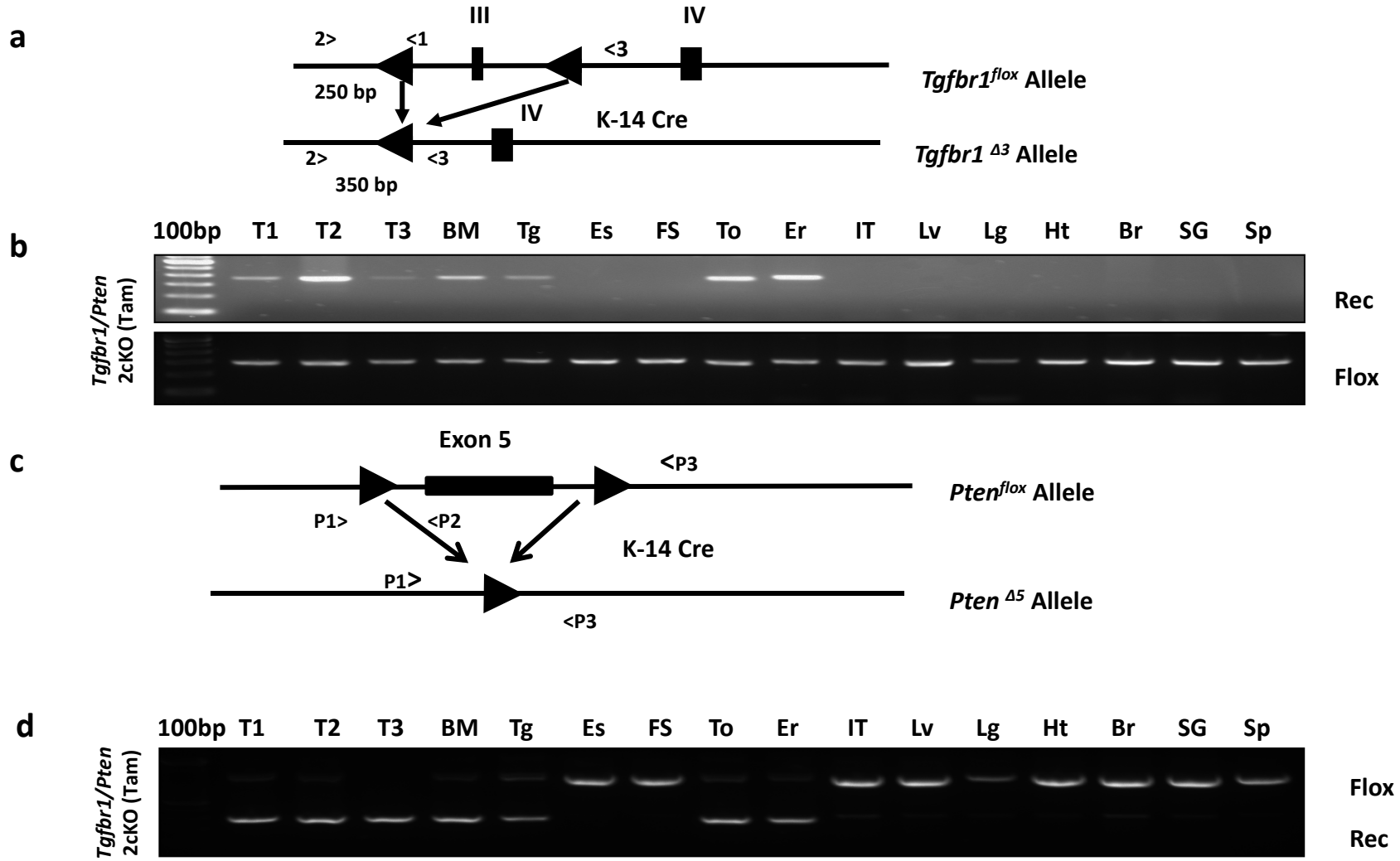

Supplemental Figure S2.

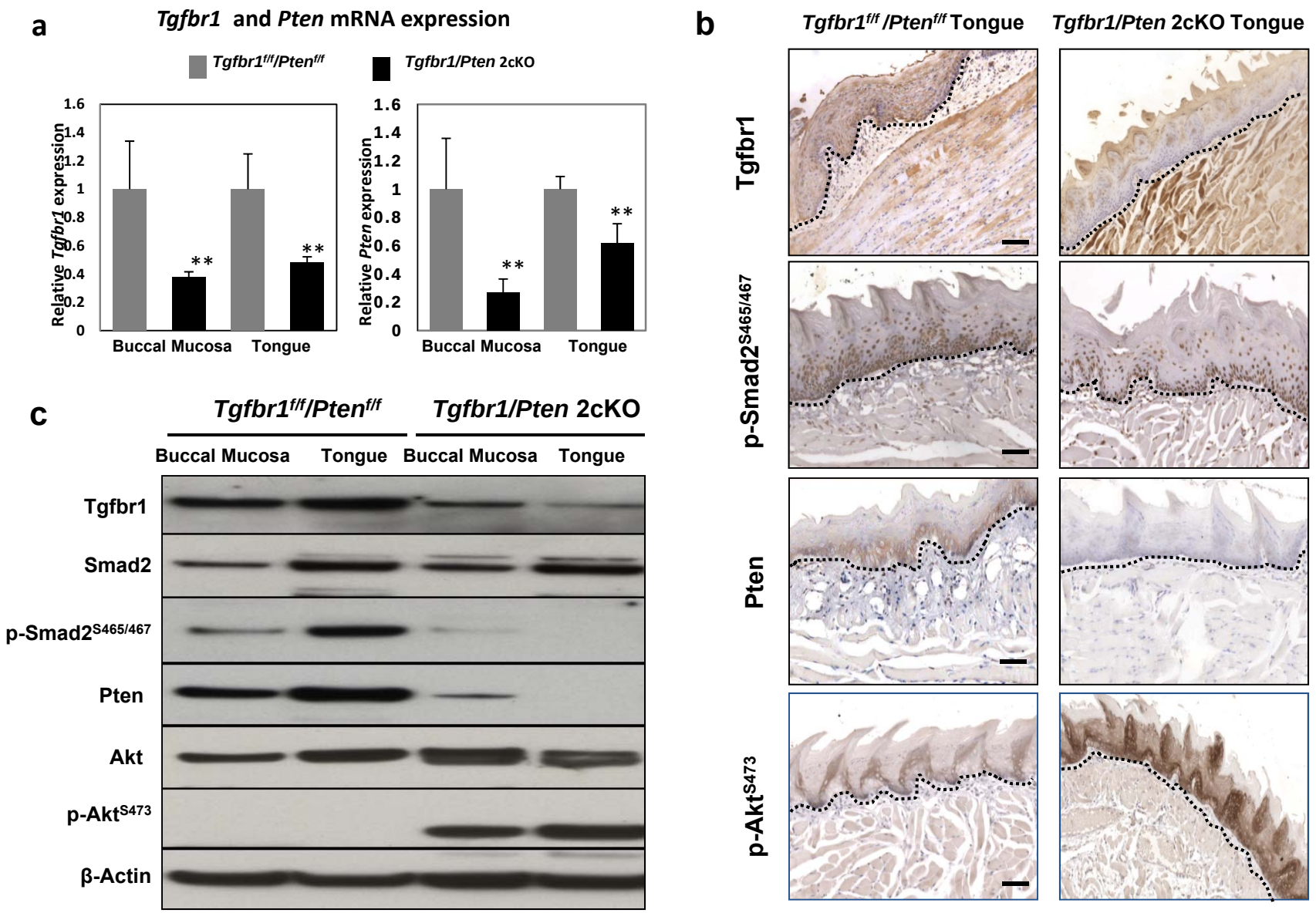

Supplemental Figure S3.

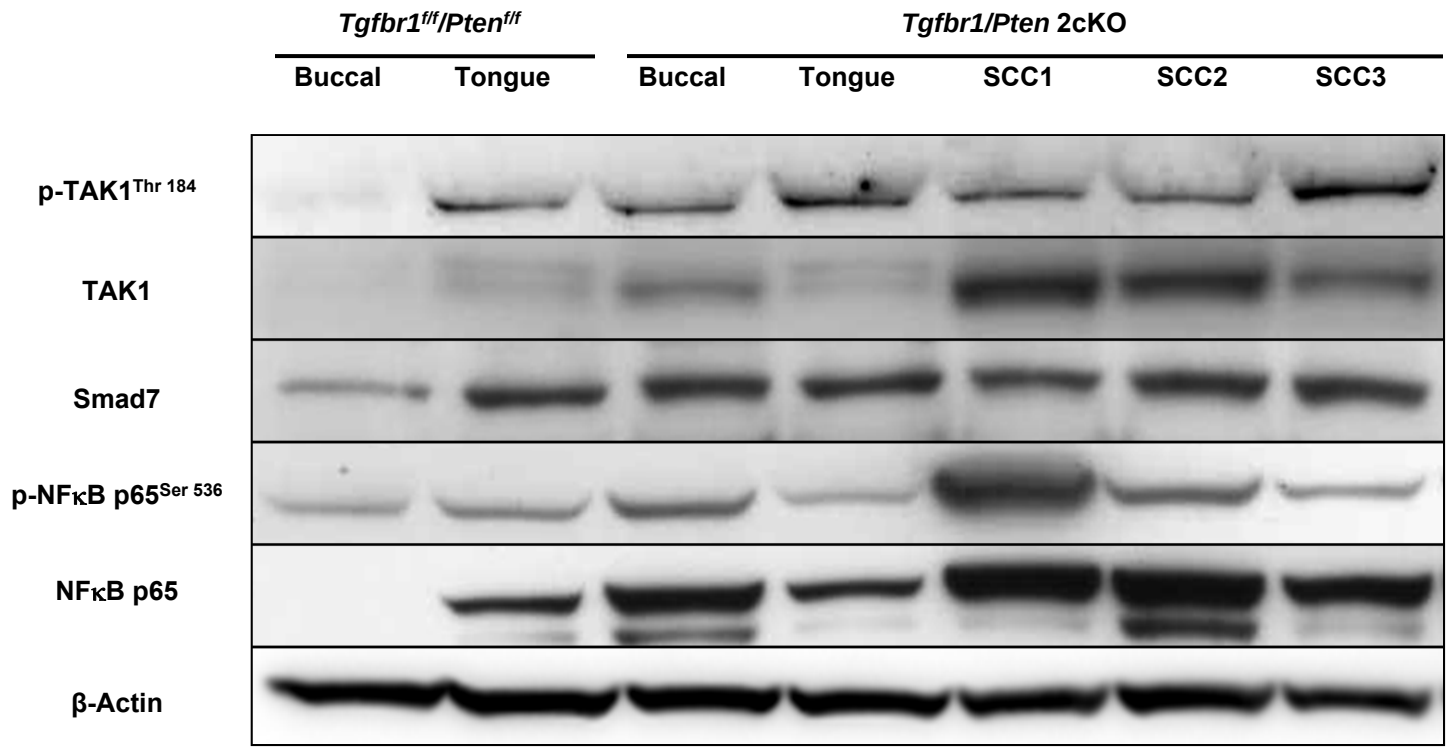

Supplemental Figure S4.

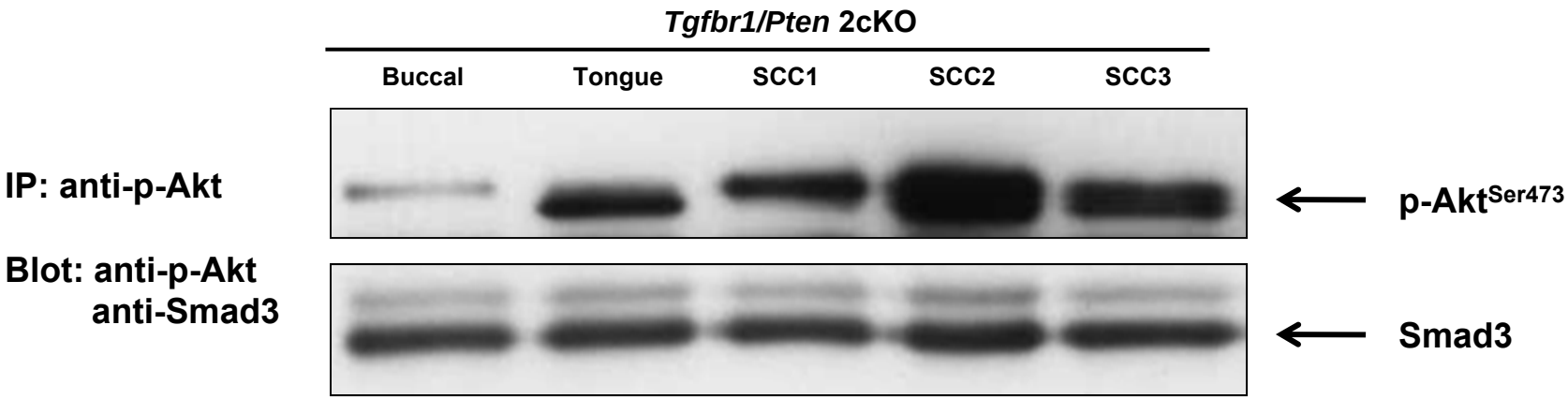

Supplemental Figure S5.

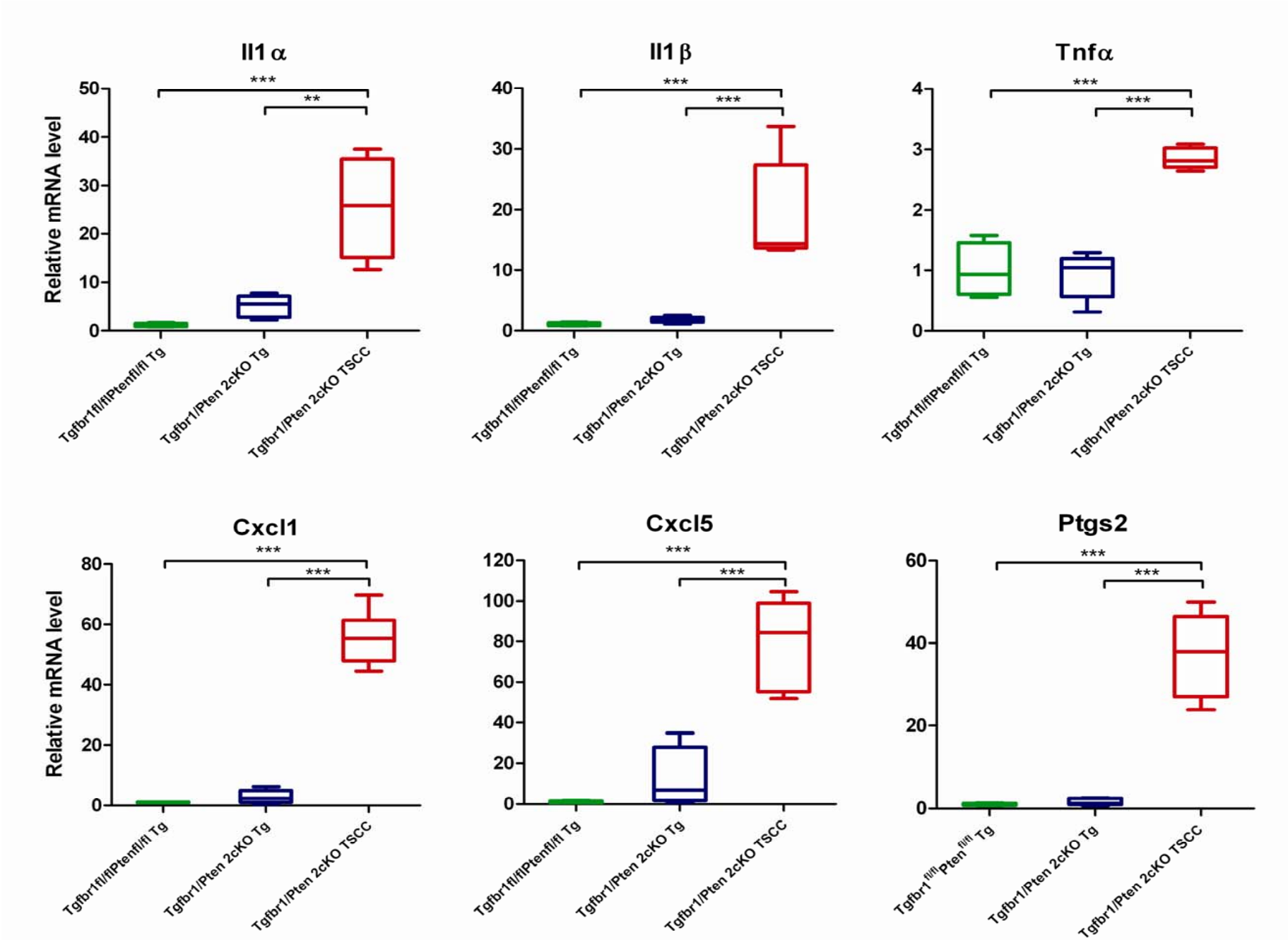

Supplemental Figure S6.

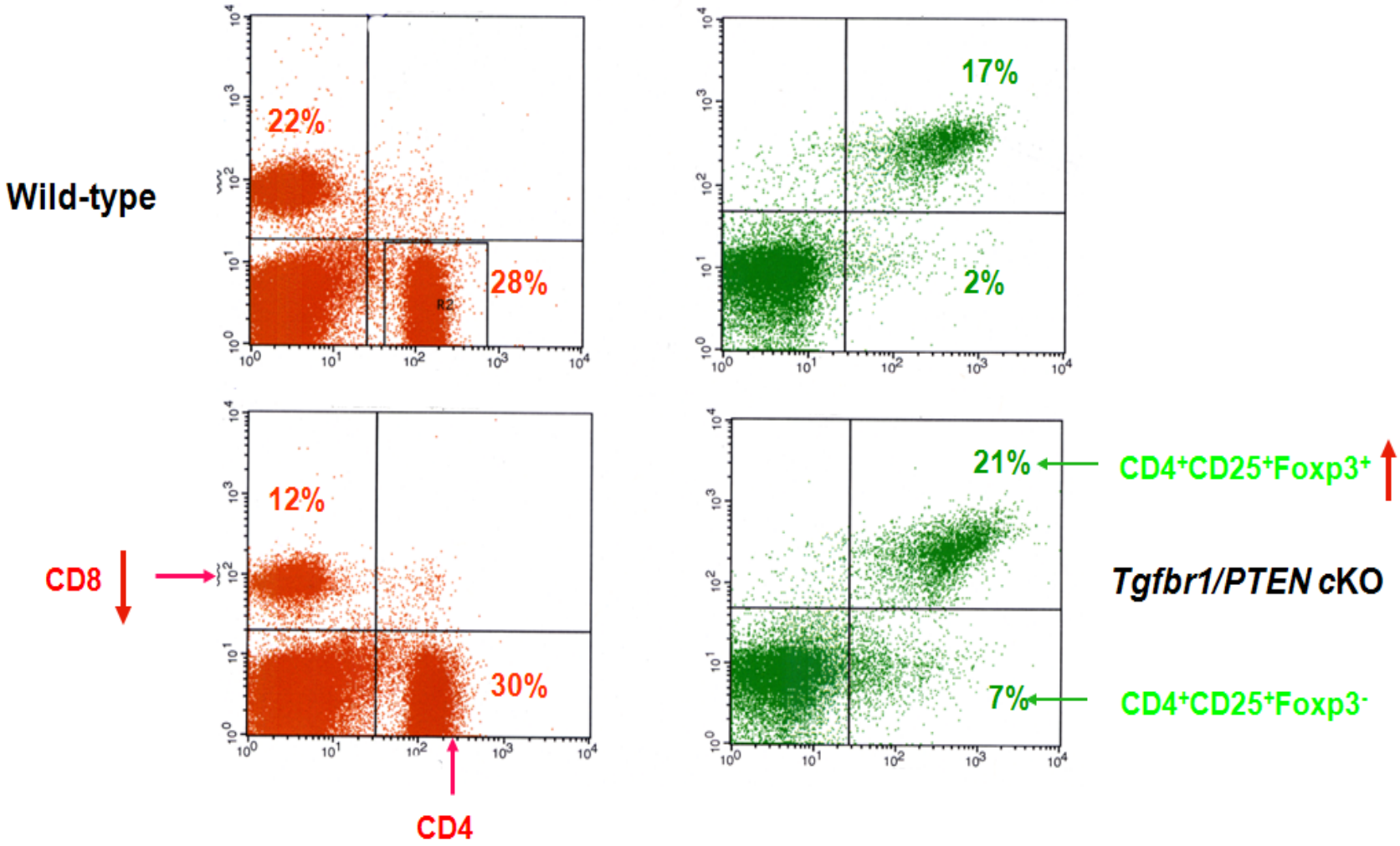

Supplemental Figure S7.